ACS APPLIED MATERIALS & INTERFACES

Research Article

www.acsami.org

Probing the Role of Carbon Microstructure on the Thermal Stability and Performance of Ultrathin (<2 nm) Overcoats on $L1_0$ FePt Media for Heat-Assisted Magnetic Recording

Shreya Kundu,[†] Neeraj Dwivedi,[†] Nalam Satyanarayana,[†] Reuben J. Yeo,[†] Joachim Ahner,[‡] Paul M. Jones,[‡] and Charanjit Singh Bhatia*[,†]

[†]Department of Electrical and Computer Engineering, National University of Singapore, 21 Lower Kent Ridge Road, Singapore 117583, Republic of Singapore

[‡]Seagate Technology LLC, Media Research Center, Fremont, California 94538, United States

ABSTRACT: An understanding of the factors influencing the thermal stability of ultrathin carbon overcoats (COCs) is crucial for their application in heat-assisted magnetic recording (HAMR) at densities ≥ 1 Tb/in^2. Two types of non-hydrogenated ultrathin (~1.5 nm) COCs were investigated after being subjected to laser-induced localized heating (at temperatures > 700 K) as envisaged in HAMR. Filtered cathodic vacuum arc (FCVA)-processed carbon with tuned C^+ ion energies of 350 eV followed by 90 eV provides significantly higher sp^3 C−C hybridization than magnetron sputter deposition even at very low thicknesses of ~1.5 nm. As a result, the FCVA-deposited ultrathin carbon overcoats displayed excellent thermal stability along with improved wear and corrosion resistance. On the other hand, the sputtered carbon exhibited carbon loss and topographical and structural changes after laser irradiation owing to lower sp^3 hybridization. Therefore, this study highlights the pivotal role of carbon microstructure, primarily sp^3 hybridization, in non-hydrogenated carbon overcoats to maintain excellent thermal stability during the recurring high-temperature cycles in a HAMR process.

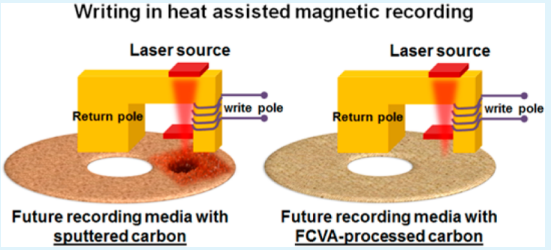

KEYWORDS: *thermal stability, ultrathin carbon, sp^3 hybridization, heat-assisted magnetic recording, filtered cathodic vacuum arc, Curie temperature*

1. INTRODUCTION

Advanced recording schemes in magnetic data storage are being widely researched due to the onset of the superparamagnetic limit at ultrahigh areal densities of ≥1 Tb/in^2.[1] Among the many technologies being studied, heat-assisted magnetic recording (HAMR) is a potential candidate for circumventing the magnetic trilemma posed by superparamagnetism and further extending the areal density in hard disk drives (HDD).[2,3] HAMR requires the use of high-anisotropy materials such as $L1_0$ FePt (K_u ≈10^7 ergs/cm^3) as the next-generation storage medium.[4,5] This allows formation of thermally stable magnetic grains with a diameter ≈ 3−4 nm. However, laser-induced localized heating of the disk surface in HAMR may affect the structural, topographical, and functional response of the protective carbon overcoats (COCs). Hence, this calls for development of COCs which can withstand localized heating when bits are being written into the media.[2]

A ~3 nm thick diamond-like carbon (DLC) overcoat protects conventional recording media surfaces from corrosion and provides good wear and scratch resistance.[6] The presence of sp^3 C−C hybridization in the COC gives it essential diamond-like character. To achieve higher areal densities, the magnetic spacing between the read/write head and the recording medium must be reduced. This, in turn, necessitates a decrease in the thickness of the COC (<2 nm) without compromising its performance. However, it is challenging to obtain adequate corrosion protection and wear resistance from <2 nm thick commercial COCs, which are typically grown using the sputtering or plasma-enhanced chemical vapor deposition (PECVD) technique.[7,8]

COCs which are deposited by the filtered cathodic vacuum arc (FCVA) technique have demonstrated better tribological and corrosion performance than those grown using the aforementioned conventional methods.[9,10] By tuning the energy of the C^+ ions in a FCVA process, ultrathin COCs (<2 nm) are attained which display continuity and high sp^3 hybridization.[11] The properties of FCVA-processed COCs can be further enhanced by employing a bilevel modification process.[12] In this process, atomic mixing of the C^+ ions with the host magnetic atoms creates a mixed layer, which is then followed by a protective film consisting of a few monolayers of C atoms.

Currently, one of the most challenging aspects in HDD is to develop thermally stable ultrathin overcoats for HAMR

Received: August 14, 2014
Accepted: December 8, 2014
Published: December 8, 2014

application. Such overcoats should display sufficient robustness to high peak temperatures and recurring thermal cycles.[13−15] Current COCs, deposited by PECVD, are mainly comprised of hydrogenated carbon (CH_x). Recent studies have shown that these overcoats degrade when they are subjected to HAMR-like conditions, such as rapid thermal annealing and localized heating.[14,15] Since the media temperature rises to 600−700 K, hydrogen is easily depleted from the carbon−hydrogen skeleton present in CH_x overcoats.[2,14] Subsequently, rearrangement occurs in the bonding of the carbon atoms and leads to increased graphitization/aromatization of the carbon network. The COC layer becomes more susceptible to corrosion and oxidation, thereby diminishing its thickness.[15−17] The presence of higher sp^3 carbon bonding in the COC is essential for enduring the recurring high-temperature cycles in HAMR.[16,18] FCVA-processed COCs are expected to have higher sp^3 carbon bonding even at lower thicknesses. In addition, these COCs do not possess any intended hydrogen in their structure. Therefore, these FCVA-processed COCs have the capability to display higher thermal stability, which is essential for HAMR application.[6,8] Moreover, recently, Samad et al.[19] used conductive atomic force microscopy to show that FCVA-modified FePt surfaces are more stable and less conductive than commercial media overcoats after laser-induced heating. Pathem et al. also showed that FCVA-processed COCs exhibit higher thermal stability than PECVD-processed COCs.[18] However, these works did not follow the exact HAMR-like conditions.

Most of the studies examining COCs (∼2−5 nm) for HAMR application did not take into account all the essential conditions, namely, rapid localized heating of the overcoat surface to the Curie temperature (T_c) at a rate close to 10^{11} K/s.[2] The few studies which did consider all the necessary conditions for HAMR were mainly focused on PECVD-based CH_x COCs.[15] There has been little or no emphasis on the localized heating of COCs grown using methods other than PECVD. Here, a significant body of work was carried out with emphasis on the following aspects: (a) ultrathin (<2 nm) and non-hydrogenated COCs deposited atop $L1_0$ FePt films using the FCVA technique and dc magnetron sputtering were investigated for thermal stability; (b) an optical pump−probe method emulating conditions foreseen in the next-generation HAMR-based HDDs such as heating temperature > T_c and a relatively rapid heating rate of 10^6 K/s was used for studying the localized changes in ∼1.5 nm thin COCs (heating rate in a HAMR-based drive should ideally be 10^{11} K/s; however, this could not be achieved with the current design of the optical set up);[15] (c) the performance of these COCs was studied on a fully structured $L1_0$ FePt media to ensure that the thermal properties studied are close to reality. It was observed that FCVA-processed COC performed better than the sputtered COC even at thickness of ∼1.5 nm.

2. EXPERIMENTAL DESIGN

A FePt media structure exhibiting perpendicular anisotropy was used for the experiment. Deposition was carried out in a magnetron sputtering (AJA Inc.) system maintained at a base pressure of 5×10^{-9} Torr. Argon was used as the sputtering gas. Ten nanometer thick FePt was grown on predeposited CrRu (20 nm)/MgO (3 nm) layers. The first underlayer, i.e., CrRu, was grown on a 1 mm thick silicon substrate at 400 °C and 1.5 mTorr pressure. The deposition conditions of MgO matched those of CrRu. These layers aided in the heteroepitaxial growth of (001) $L1_0$ FePt. The FePt layer was grown at 600 °C and 3 mTorr pressure to achieve the $L1_0$ ordering.[20]

For the first set of FePt samples, 1.5 nm thick carbon films were sputter deposited at room temperature and 3 mTorr pressure. This set of samples is referred to as SC I. The second set of FePt samples, denoted as FC I, was subjected to bilevel surface modification employing the FCVA technique. The FePt magnetic medium was first bombarded with energetic C^+ ions at 350 eV to form a mixed layer. This was followed by a lower energy deposition step at 90 eV such that an ultrathin COC with high sp^3 hybridization was obtained.[12] To achieve the required ion energies, the substrate was negatively biased. Negative pulsed voltages of 340 and 80 V, at a frequency of 20 kHz and duty cycle of 60%, were applied. The thickness of the COCs in the SC I and FC I sets was equal to and maintained at ∼1.5 nm.

An optical pump−probe setup was used for irradiating the sputtered (SC I) and FCVA (FC I) grown carbon films. Figure 1a shows the

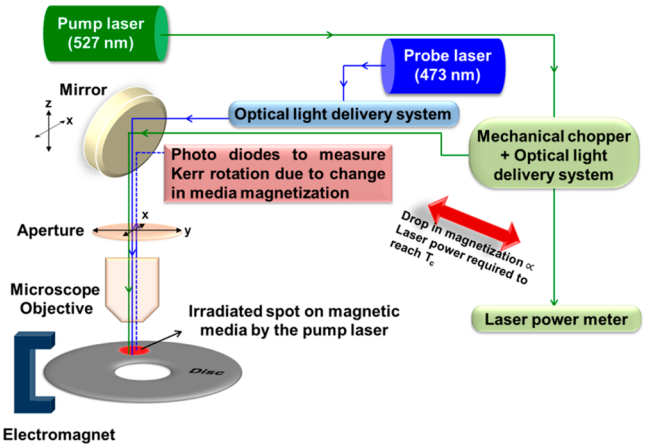

Figure 1. Schematic of the optical pump−probe setup used at Seagate.

schematic and working principle of the optical pump−probe station. It consists of a pump laser (λ = 527 nm) to locally heat the overcoat-protected media. The irradiated spot was ∼8 μm in diameter. The magnetization of the media changed with increasing temperature and was detected by a second probe laser (λ = 476 nm). This allowed determination of the pump power required to attain T_c, the temperature at which magnetization becomes zero, at the selected spot on the media. A peak temperature > 700 K was used for $L1_0$ FePt. On the basis of the power and its gradient in the neighboring regions, the response of the COCs to high heating rates (∼10^6 K/s) and smaller dwell times (500 μs) was studied. The total heating time was 2 s. In essence, the pump−probe setup simulated the possible HAMR configuration as envisaged for future HDDs closely. Such a setup is beneficial for comparing any localized changes in the topography and microstructure of COCs at the micrometer-sized heated spot with respect to the unheated surroundings. Angle-resolved X-ray photoelectron spectroscopy (ARXPS) was used to characterize the chemical bonding present in the two types of COCs: SC I and FC I. ARXPS measurements were performed at a photoelectron take-off angle of 25° (0° being parallel to the surface) using a VG ESCALAB 220I-XL spectrometer with an Al Kα source. Ultraviolet (UV) Raman spectroscopy measurements were carried out using a Jobin Yvon LABRAM-HR spectrophotometer. An excitation wavelength of 325 nm from a He−Cd laser was used. The laser power used during the measurement was kept low in order to avoid any damage to the ultrathin COCs. The relative intensity ratios of the peaks obtained from different locations of the COCs were compared to examine the nature of the carbon bonding with an accuracy of <2%. The tribological properties of these overcoats were evaluated using a nanotribometer (CSM Instruments) in ball-on-disk sliding mode. A sapphire ball of 2 mm diameter was used as the counterface. Sliding tests were conducted by employing a normal load of 20 mN, a radius of rotation of 1.2 mm, and a sliding velocity of 1.0 cm s^{-1}.

dx.doi.org/10.1021/am5054724 | ACS Appl. Mater. Interfaces 2015, 7, 158−165

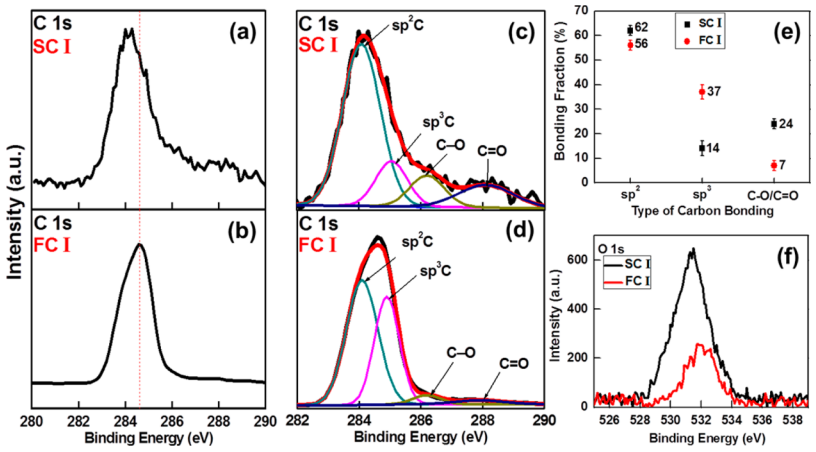

Figure 2. ARXPS C 1s core level spectra of samples (a) SC I and (b) FC I. Deconvoluted C 1s core level spectra of samples (c) SC I and (d) FC I. (e) Plot of % bonding fractions of sp^2C, sp^3C, and C−O + C═O for samples SC I (black squares) and FC I (red circles). (f) ARXPS O 1s core level spectra of samples SC I and FC 1. ARXPS measurements were performed at a photoelectron take off angle of 25°.

3. RESULTS AND DISCUSSION

A thorough study investigating the chemical bonding of carbon to its immediate environment is necessary to analyze the thermal stability of SC I and FC I overcoats. Hence, to examine the bonding environment of carbon in samples SC I and FC I, ARXPS measurements were performed using a photoelectron take-off angle of 25° (Figure 2). Figure 2a and 2b shows the C 1s core level spectra obtained from the COCs in samples SC I and FC I, respectively. The C 1s peak in sample FC I appeared to be shifted toward higher binding energies when compared to SC I. The peak position for diamond-like sp^3C bonding is present at higher binding energy with respect to graphite-like sp^2C bonding. Hence, it can be concurred from the C 1s spectra of the two types of COCs that sample FC I has relatively higher sp^3C bonding than sample SC I. In order to comprehensively investigate the bonding environment of carbon in these samples, the C 1s spectra of these samples were deconvoluted with various Gaussian components after Shirley background subtraction. Figure 2c and 2d shows the deconvoluted C 1s core level spectra of samples SC I and FC I. The deconvoluted C 1s spectra of both samples show four peaks at 284.1, 285.0 ± 0.05, 286.2, and 288.0 ± 0.1 eV, which are attributed to sp^2C, sp^3C, C−O, and C═O bonding, respectively.[9,21−23] The area ratio method is then used to quantitatively determine the fractional contributions of different carbon bonding to C 1s spectra of each sample (Figure 2e). It is evident from Figure 2e that FC I has significantly higher sp^3C bonding (~37%) than sample SC I (~14%). Apart from higher sp^3C bonding, FC I showed a considerably lower amount of bonding of carbon to O (C−O + C═O). The O 1s core level spectra of the two samples have also been shown in Figure 2f to examine the interaction of ambient oxygen or water vapor with COCs during the storage time between deposition and ARXPS characterization of these samples. The amount of oxygen present on the surface of FC I was lower when compared to that on SC I. Lesser oxygen on the sample surface ensured minimal carbon−oxygen bonding in FC I than present in SC I, which is further confirmed by C 1s core level spectra. The lower interaction of oxygen with COC in FC I than SC I was due to higher oxidation resistance provided by FCVA-processed COC owing to its higher sp^3 bonding and density. This is crucial as the underlying magnetic media will also be protected from oxidation/corrosion. Thus, ARXPS analysis on these two samples suggested that FCVA-processed COC has two important characteristics: (1) higher sp^3C bonding and (2) lesser interaction of oxygen with carbon. Higher sp^3C content is beneficial for the thermal stability of the overcoat as will be shown in a following section, while lesser carbon−oxygen interaction is useful for protection from oxidation and corrosion of underlying recording layer.

A combination of atomic force microscopy (AFM) and Raman spectroscopy was utilized in observing and understanding the changes in the topographical and structural properties of the two types of COCs before and after laser irradiation. Figure 3 shows the two-dimensional AFM images

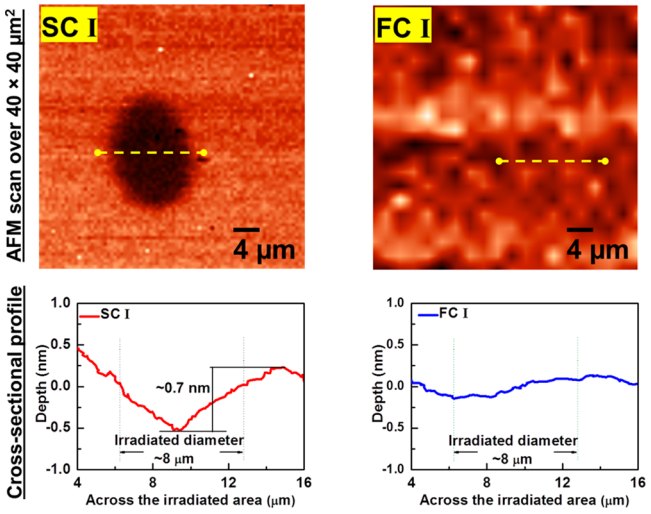

Figure 3. Two-dimensional AFM scans (top) and cross-sectional profiles (bottom) carried out on surfaces of SC I and FC I. Yellow dotted line shows the direction along which the cross-sectional profiles were acquired.

and cross-sectional profiles of SC I and FC I after laser irradiation. SC I was locally heated to 764 K for 2 s (which is on the order of the total heating time of a given spot on the media during the mean lifetime of a HAMR-based HDDs[14]), resulting in formation of a ~8 μm wide and ~0.7 nm deep hole on SC I. Nearly one-half of the COC thickness was lost at the irradiated region. On the other hand, the AFM scan and cross-sectional

dx.doi.org/10.1021/am5054724 | ACS Appl. Mater. Interfaces 2015, 7, 158−165

profile carried out on FC I , after laser irradiation at 790 K for 2 s, did not show any significant variation in the surface topography. Therefore, FC I did not exhibit any COC thickness loss.

High-resolution, visible nano-Raman spectroscopy was employed to understand the mechanism underlying the thinning of the sputtered COC. The spectrometer, operating at a wavelength of 448 nm, is able to map the total intensity of the Raman peaks obtained over an area of 100 × 100 μm^2. Furthermore, the spectral and spatial resolution of the equipment helped to differentiate between any changes in the peak positions and intensities acquired at closely spaced measurement points on the overcoat surface. Since SC I underwent topographical damage upon laser irradiation (Figure 3), Raman measurements were performed at three different locations on SC I (Figure 4a–d): the nonirradiated region (location 1), inside the irradiated region (location 2), and the periphery of the irradiated region (location 3). Raman measurements were also carried out on FC I for comparison. The insets in Figure 4a show the two-dimensional AFM image of SC I and FC I. The images show the locations where Raman spectroscopy was performed on SC I. Raman spectra of these samples were fitted using various functions (BWF, Gaussians, and Lorentzians). The best fit to the spectra was obtained with Lorentzians. Therefore, all spectra were fitted using two Lorentzians except for the spectra recorded at the periphery of sample SC I where three Lorentzians were used. Three Loretzians were used for fitting the Raman spectra of SC I at the periphery because the area between D and G peaks was flat, indicating the contribution of other carbon phases. Raman spectra of samples SC I and FC I, which were fitted with two Lorentzian components (Figure 4b–e), showed the D peak (A_{1g} breathing modes of sp^2 bonded carbon atoms in rings) and G peak (E_{2g} symmetrical bond stretching motion of all pairs of sp^2 bonded carbon atoms in both rings and chains) of amorphous carbon.[24−26] Figure 4b–e shows the fitted Raman spectra carried out on the three locations on SC I and FC I. For the benefit of the readers, the three-dimensional AFM images of the overcoat surfaces have also been presented as insets in Figure 4b–e. The yellow dot on each image depicts the spot from where the Raman spectrum was recorded. Figure 4f compares the G peak positions of FC I to those attained at different locations on SC I. In order to study the structural changes in the COCs before and after localized irradiation, the intensity ratios of the decomposed D to G peaks (I_D/I_G) for the two sets are compared in Figure 4g.

Visible Raman spectroscopy is predominantly sensitive to sp^2 hybridization in a carbon network. Manifestation of any ordering–disordering, sp^2 clustering, and change in sp^2 bonding in the COC can be identified from deviations in the G peak position and I_D/I_G ratio. The results on sputtered COC are presented first, which are then followed by those attained on FCVA-processed COC. The G peak from location 1 on SC I was seen at ∼1555 cm^{-1} (Figure 4b and 4f), near the G peak position in amorphous carbon.[24] Hence, it was suggested that prior to irradiation the COC in SC I was rich in sp^2 bonding.[24] Ferrari and Robertson proposed a three-stage model for amorphous carbon films consisting of different sp^3 and sp^2 bonding fractions.[24] The G peak from the nonirradiated region of the COC in SC I appeared in the second stage of the model (sp^3 < 20%). The G peak position of SC I, having a sp^3 content of ∼14% (as deduced from ARXPS), is in agreement with the G peak position of the films that were studied under the three-stage model and have a similar sp^3 content of ∼10–15%. In addition, the G peaks acquired at the irradiated (location 2, ∼1549 cm^{-1}) and nonirradiated (location 1, ∼1555 cm^{-1}) regions were in close proximity to each other (Figure 4f). In other words, the residual COC (after carbon loss) did not show any substantial change in the sp^2 bonding upon localized heating.

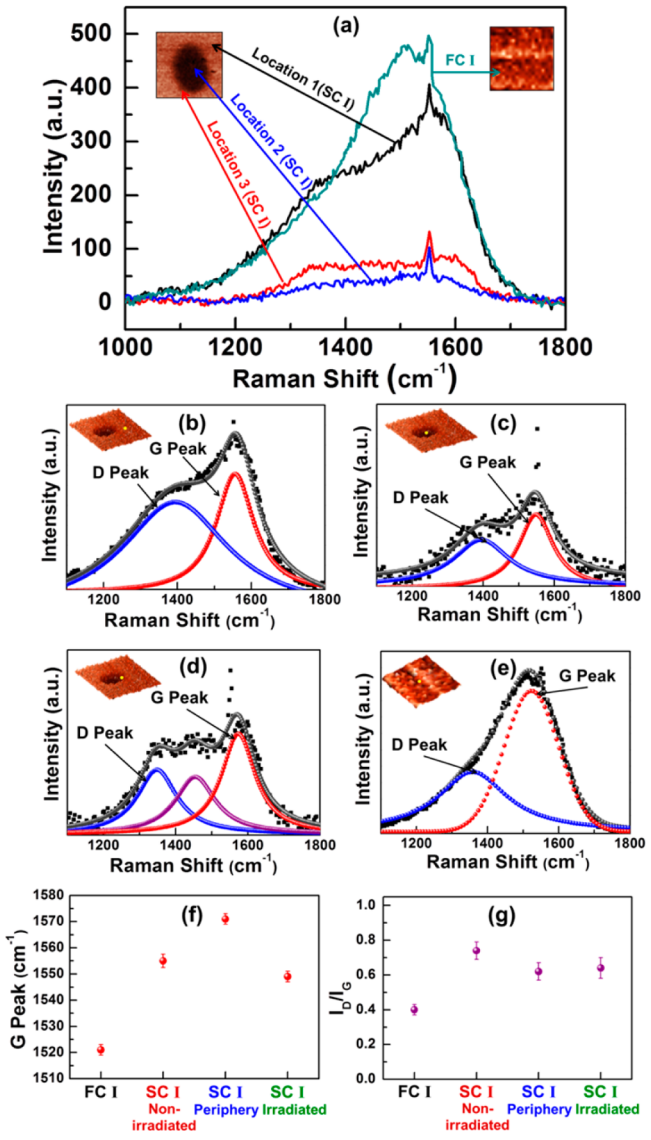

Figure 4. (a) Visible Raman spectroscopy carried out on FC I as well as on SC I at three different locations which have been indicated in the inset; (b–d) Extracted G and D peaks obtained at three locations on SC I. Yellow dot in the three-dimensional AFM images (insets) show the spots where spectroscopy was performed. (e) Visible Raman spectra carried out on the irradiated surface of FC I. (Inset) Three-dimensional AFM image of the unaffected overcoat surface after localized heating. (f) Variation in G peak positions. (g) I_D/I_G intensity ratio as a function of sample type (FC I or SC I) and the three locations on SC I.

No significant change was observed in the visible Raman spectra of FC I before and after laser-induced irradiation. The G peak position for FC I (after irradiation) was observed at ∼1521 cm^{-1} (Figure 4e and 4f). Previously, Anders et al. carried out a systematic study on FCVA-processed carbon films employing visible Raman spectroscopy.[27] In their work, it was

dx.doi.org/10.1021/am5054724 | ACS Appl. Mater. Interfaces 2015, 7, 158–165

shown that a G peak position of ~1520 cm^{-1} in amorphous carbon films corresponded to ~39% sp^3 bonding. In accordance with Ferrari and Robertson's three-stage model for amorphous carbon films, the G peak position acquired from FC I appeared at the beginning of the third stage (~35% sp^3 bonding).[24] Furthermore, Yeo et al.[12] used the same FCVA-based bilevel surface modification technique, i.e., embedment at 350 eV followed by 90 eV on CoCrPt-based magnetic media to achieve sp^3 bonding of ~41% in the COC. All these studies clearly suggest that the COC in FC I probably contained sp^3 hybridization of ~35−40%, which is much higher than SC I.[12,24,27] The full-width half-maxima (fwhm) of the G peak evaluated from the visible Raman spectra of the FC I overcoat (Figure 4e) was significantly higher than that of SC I (Figure 4c). This also reinforces the fact that FC I possessed higher sp^3 bonding than SC I.[24]

In order to further assess the microstructure of these COCs in terms of sp^3 and sp^2 carbon bonding, UV Raman measurements were performed on SC I and FC I. Figure 5a shows the UV Raman spectra of bare FePt, SC I, and FC I. UV Raman spectra were fitted and plotted again for SC I and FC I as shown in Figure 5b and 5c, respectively. Since bare FePt has no COC, D and G peaks corresponding to the carbon film were not observed in the range of 1000−1800 cm^{-1}. On the other hand, the COCs in SC I and FC I exhibited both D and G peaks. Spectra upon being fitted with Lorentzian peaks showed a G peak position at 1589 cm^{-1} for SC I and 1582 cm^{-1} for FC I. The G peak positions were analyzed in view of the three-stage model, and the results showed that the G peak of FC I lies in the third stage and is expected to have sp^3 bonding in the range of ~35−40%. In contrast, the G peak of SC I appeared in the middle of the second stage with sp^3 bonding present in the range of 10−15%, consistent with visible Raman results. Moreover, the G peak fwhm in UV Raman spectra was also found to be considerably higher in FC I than in SC I, which further reinforced the fact that FC I has relatively higher sp^3C hybridization. Furthermore, it is known that the G peak, as a function of excitation wavelength, does not disperse in graphite or nc-graphite (pure sp^2-bonded carbon network), while it disperses significantly when carbon films possess significant sp^3 bonding.[24] It is seen from visible (448 nm) and UV (325 nm) Raman spectra that the difference of G peak position at these two wavelengths is significantly higher in FC I with respect to SC I. This further supports the fact that FC I has significantly higher sp^3 bonding than SC I. Thus, localized heating of 2 s above the Curie temperature (~700 K) and rapid thermal cycles had no significant effect on the FCVA-grown COC due to the presence of higher sp^3 bonding.

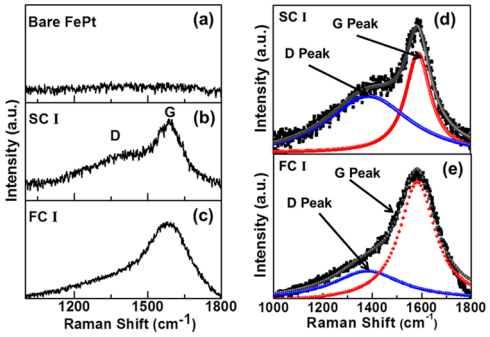

Figure 5. UV Raman spectra of samples (a) bare FePt, (b) SC I, and (c) FC I. Fitted UV Raman spectra of samples (d) SC I and (e) FC I.

The excellent thermal stability observed in FC I compared to SC I is expected mainly due to the higher sp^3 content in FC I. One of the reasons for poor thermal stability of the previously studied CH_x-based COCs is the effusion of hydrogen from the C−H skeleton at higher temperatures. In our work, we examined two non-hydrogenated COCs. Therefore, the role of hydrogen on the thermal stability of COCs in FC I and SC I can be ruled out. In addition, any influence of the overcoat thickness on their thermal stability can also be eliminated since FC I and SCI consisted of COCs of similar thicknesses. The substrate atop which these two ultrathin, non-hydrogenated overcoats were deposited, i.e., the FePt media stack, was also identical. Hence, the media material can also not be accounted for observing higher thermal stability in FC I than in SC I. In other words, the differences present in the carbon microstructure in FC I and SC I is the only factor producing a variation in their thermal stability. FC I has higher sp^3 bonding (~35−40%) than SC I (~10−15%). Thus, the higher sp^3 bonding enhances the thermal stability of FCVA-processed COC in FC I. There have been several systematic studies on the thermal stability of non-hydrogenated carbon films to support our argument. Kalish et al. reported that the thermal stability of carbon films is directly proportional to the sp^3 bonding present in them.[28] Carbon films with ~80% sp^3 bonding are stable upon annealing and do not graphitize up to 1073 K, while carbon films with ~40% sp^3 bonding are stable up to 723 K upon annealing for 30 min. Ferrari et al. also reported that higher sp^3-bonded carbon (~87%) films can be thermally stable up to 973 K.[29]

COCs grown using the in situ FCVA technique (FC I) displayed higher sp^3 bonding than the sputtered COCs (SC I) due to the difference in the energetics associated with the two deposition processes. FCVA generates highly ionized plasma of C^+ ions whose energy can be tuned by varying the substrate bias. The incident ions of adequate energies penetrate the surface of the growing films, causing subsurface growth, which enhances the local density. This process, known as subplantation, helps in attainment of higher sp^3 bonding in FCVA-processed carbon films.[30,31] The optimum ion energy for achieving maximum sp^3 bonding in a carbon layer is ~90−100 eV.[31] Since embedment at 350 eV was followed by 90 eV in the bilevel modification technique, a dense and sp^3-rich carbon layer was expected to form in FC I. On the other hand, the plasma generated during sputtering consists mainly of the low-energetic and unionized species. The sputter-deposited COC was formed from low-energy C atoms (<5 eV), which were unable to penetrate the surface and, hence, would lead to formation of films with mainly sp^2 bonding. Deposition of carbon films by sputtering has an energetic distribution of median < 5 eV. However, a high-energy tail of ≥40 eV can exist.[32] Therefore, the process is a superposition of surface-deposited carbon atoms and a few energetic subplanted atoms. This can cause the sputtered COC (in SC I) to possess a small amount of sp^3-bonded carbon atoms. Overall, the carbon layer in SC I is richer in sp^2 hybridization than sp^3 hybridization.[31]

Intensity measurements of the G peaks are useful for mapping the extent of oxidation at the three different locations on SC I. While carrying out visible Raman spectroscopy, a sharp drop in the intensity of the G peak was obtained at the irradiated spot (~60 au, Figure 4c) when compared to that at the nonirradiated spot (~400 au, Figure 4b). The Raman

dx.doi.org/10.1021/am5054724 | ACS Appl. Mater. Interfaces 2015, 7, 158−165

spectrometer and system parameters were kept constant throughout the measurements. Also, measurements were carried out on different locations of the same sample sequentially. Hence, the diminished intensity attained at the irradiated spot (location 2) was only due to the COC loss from oxidation. The AFM cross-sectional profile of SC I in Figure 3 supports this argument. Oxidation of the SC I overcoat due to localized heating resulted in formation of a cavity (Figure 3). The immediate region surrounding the irradiated spot on the COC (location 3) also underwent carbon loss (Figure 4d). A G peak intensity of ∼90 au was observed, which is almost similar to the intensity of the G peak recorded at the center (∼60 au). The periphery of the irradiated spot displayed slightly lower carbon loss and oxidation than the irradiated region as the intensity of the G peak at the periphery was slightly higher (by ∼30 au). This variation was most likely due to the existence of a temperature gradient across the irradiated spot. Interestingly, at the periphery of the irradiated spot the G peak position was seen at ∼1571 cm^{-1} (Figure 4d and 4f). This indicated the occurrence of graphitization as the Raman G peak of graphite and nanocrystalline graphite varied between 1580 and 1600 cm^{-1}.[24] Compared to the nonirradiated and irradiated regions on SC I (Figure 4b, 4c, and 4f), the sp^3 bonding at the periphery decreased and approached zero (Figure 4d and 4f). Marginally lower temperature at the periphery reduced the oxidation rate of the carbon layer slightly. However, the temperature was sufficient to induce graphitization. Similar carbon loss by localized heating was previously observed for PECVD-based CH_x COC at greater thicknesses of 5 ± 2 nm.[15] Apart from the D and G peaks, the Raman spectra of SC I at periphery displayed an additional peak at ∼1455 cm^{-1}. This peak might be due to the superposition of different carbon phases from nonirradiated and irradiated regions at the periphery. The 1.5 nm thick and sp^3-rich COC grown using the FCVA technique in FC I displayed a high G peak intensity of ∼500 au and no indication of graphitization or oxidation—overcoat properties crucial for ensuring thermal stability under HAMR-like conditions.

For amorphous carbon materials, the I_D/I_G ratio can be a measure of ring-like sp^2 cluster formation (Figure 4g). The COC in FC I displayed an I_D/I_G ratio of ∼0.4 after localized heating. This is much lower than the ratio attained at the nonirradiated region on SC I (∼0.74). A low sp^3 content (∼10−15%) in SC I suggests that the microstructure of this COC consisted mainly of sp^2 sites. The large I_D/I_G ratio indicates that these sites were puckered into disordered ring-like networks. A few sp^3 sites might also be present within the carbon network. In contrast, a lower I_D/I_G ratio in FC I indicated a lower amount of ring-like sp^2 clustering within the carbon network. In SC I, the I_D/I_G ratio was found to be similar at the periphery (∼0.62) and at the irradiated spot (∼0.64) (Figure 4g). Unexpectedly, the I_D/I_G ratio was found to be slightly smaller at the irradiated spot than at the nonirradiated region. The difference in the ratio was ∼0.1, which is considered marginal. It was earlier been discussed that the G peak positions of the irradiated and nonirradiated regions on SC I differed slightly by ∼6 cm^{-1}. This small difference between the two G peaks, both of which fall in stage 2 of Ferrari and Robertson's three-stage model, corresponded to a negligible change of ∼1% in the sp^3 bonding.[24] This suggests that the shift in the G peak position was insignificant with respect to any change in sp^3 and sp^2 bonding. It is complex to explain the observation of a slightly lower I_D/I_G ratio at the center of the irradiated spot than at the nonirradiated spot. The center of the irradiated spot underwent oxidation and COC loss upon localized irradiation. The slightly reduced I_D/I_G ratio observed at the center could be due to the occurrence of modified carbon phases. Ji et al. also showed Raman spectra of ultrathin a-CN_x, CH_x, and a-C overcoats before and after laser annealing which match closely with our results.[33] They found that the I_D/I_G ratio decreased slightly by ∼0.1 after laser-based annealing when compared to nonannealed samples with a-C:H_x and a-C overcoats. The I_D/I_G ratio was also found to be slightly lower (∼0.62) at the periphery than at the nonirradiated spot (∼0.74). This could be due to the superposition of different carbon phases from irradiated and nonirradiated spots. UV Raman results are in good agreement with visible Raman results and showed that the I_D/I_G ratio was much lower in FC I (∼0.21) than in SC I (∼0.54) prior to laser irradiation.

Besides thermal stability, the other crucial requirements for the overcoats designed for HAMR are higher wear resistance and a lower coefficient of friction (COF). An optimal value of COF helps to ward off mechanical damage to the media surface during any intermittent contact between the head and the media. Hence, ball-on-disk measurements were performed to assess the tribological performance of SC I and FC I. Figure 6a shows the frictional plots (coefficient of friction (COF) versus number of cycles) of bare FePt, FC I, and SC I. The surfaces of the three samples and the ball were observed using an optical microscope to investigate formation of any wear tracks after ball-on-disk tribological tests (Figure 6b−d). From Figure 6a, it is evident that bare FePt media exhibited a high COF (∼0.6), severe wear track, and a considerable amount of material transfer to the ball. Sputtered carbon on FePt media (SC I) displayed a change in the COF value throughout the first 2000 cycles, eventually stabilizing at ∼0.6, the same as that of bare FePt. Significant transfer of debris to the ball and a noticeable wear track were also observed in the case of SC I (Figure 6c). In contrast, a lower COF was observed for FC I during all wear cycles, which eventually led to lesser debris accumulation on the ball surface and a mildly visible wear track on the sample surface. The higher wear resistance and lower COF in FC I compared to SC I could be attributed to the significant atomic mixing between the C^+ ions and the host (Fe and Pt) atoms at 350 eV. The mixed layer created strong adhesion between the carbon layer deposited at 90 eV and the media surface. Some amount of atomic mixing is possible in sputtering due to a higher energy tail of ≤40 eV. The mixing is, however, not as large as that obtained with the FCVA process. Thus, higher sp^3

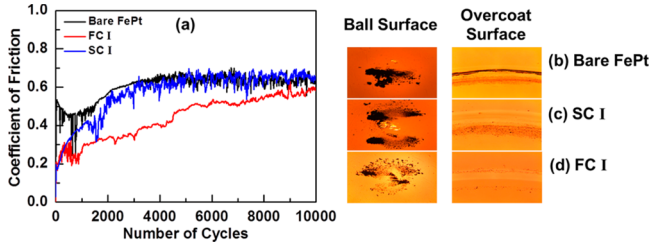

Figure 6. (a) Plot of COF versus number of cycles for bare $L1_0$ FePt media and FePt media protected by SC I and FC I overcoats. Optical images of the counterface sapphire ball and surface wear tracks after 10 000 sliding cycles are also shown for (b) bare FePt media, (c) SC I overcoat, and (d) FC I overcoat.

dx.doi.org/10.1021/am5054724 | ACS Appl. Mater. Interfaces 2015, 7, 158−165

bonding and improved adhesion due to higher atomic mixing lead to the higher wear resistance in FC I than SC I.

In a 4-fold-coordinated sp^3-hybridized network, each carbon atom forms strong σ bonds with adjacent carbon atoms, which provides rigidity to the overall carbon network. However, a 3-fold-coordinated sp^2-hybridized network contains a weaker π bond in addition to σ bonds. The presence of a weaker π bond lowers the rigidity of the carbon network in the sp^2 configuration, thereby making it prone to oxidation and mechanical wear. This was clearly demonstrated by comparing FC I with SC I. Hence, the presence of higher sp^3 bonding in COCs is the key determinant for obtaining higher thermal stability and higher wear and corrosion resistance.[12] Moreover, the thermal conductivity of an amorphous carbon film increases with increasing sp^3 hybridization.[34,35]

The sp^3 bonding of amorphous carbon scales proportionally with density (ρ) of the film as given in eq 1

$$\rho(\mathrm{g/cm^3}) = \rho_{\mathrm{Graphite}} + \mathrm{sp^3}(\rho_{\mathrm{Diamond}} - \rho_{\mathrm{Graphite}}) \quad (1)$$

Using the above relation and sp^3-bonding content of FC I and SC I, ρ of the COCs in SC I and FC I was estimated. The value of ρ for COC in SC I was found to be ~2.38 g/cm^3. The value of ρ increased to 2.68 g/cm^3 for COC in FC I. The values of ρ_{Graphite} and ρ_{Diamond} used were 2.2 and 3.5 g/cm^3. Furthermore, from eq 2 it can clearly be seen that the thermal conductivity K, measured using the 3ω method, is proportional to ρ of the carbon film.[31]

$$K[\mathrm{W/mK}] = 1.77\rho[\mathrm{g/cm^3}] - 2.82 \quad (2)$$

Using the calculated values of ρ for SC I and FC I, K was determined for these two samples. The value of K for SC I was found to be 1.4 W/mK, which increased slightly to 1.9 W/mK for FC I. In addition, the C−C sp^3 hybridization is proportional to the structural disorder in the as-deposited COCs. Structural disorder can be quantified by measuring the fwhm of the G peak at a certain wavelength

$$K[\mathrm{W/mK}] = C + A \times \mathrm{FWHM\ of\ G\ peak(cm^{-1},\ at\ a\ certain\ wavelength)} \quad (3)$$

where C and A are constants which change with variation in the wavelength of the laser used in Raman spectroscopy. From Figure 4c and 4e, the fwhm of FC I is estimated to be 1.6 times higher than SC I. Therefore, the FC I overcoat has higher thermal conductivity than SC I. Although K was higher in FC I than SC I, the difference is not significant. Moreover, the observed thermal conductivity in amorphous carbon films is much lower than crystalline diamond (which is on the order of hundreds of W/mK). Hence, the observed higher thermal stability in FC I than in SC I is mainly due to the rigid sp^3 bonding which, in turn, prevents its degradation against laser-induced localized heating. This small increment in thermal conductivity of FC I can add to the enhancement of its stability.

4. CONCLUSION

The localized heating-induced thermal stability of ultrathin (~1.5 nm) and non-hydrogenated COCs produced by FCVA and dc sputtering was investigated under HAMR-like conditions using a combination of AFM and Raman spectroscopy. The 1.5 nm thick FCVA-grown COC in FC I was determined to be thermally stable as (1) the AFM cross-sectional profile and two-dimensional scans did not show any topographical damage or COC loss and (2) Raman spectroscopy did not show any structural changes in the COC.

In contrast, sputter-deposited COC of the same thickness (~1.5 nm) in sample set SC I underwent structural and topographical damage. Significant carbon loss due to oxidation was also observed. The higher stability of FC I against laser-induced localized heating, compared to SC I, was due to the presence of higher sp^3 bonding in the FCVA-processed COC. Additionally, ball-on-disk tribological tests showed that FC I performed better than SC I, leading to a lower COF and higher wear resistance. In summary, our investigation clearly shows that the presence of higher sp^3-bonding content in COCs is essential for enduring the high temperatures, high-temperature gradients, and repeated thermal excursions present in HAMR. These findings are extremely important for development of potential COCs for HAMR application in HDDs.

AUTHOR INFORMATION

Corresponding Author

*E-mail: elebcs@nus.edu.sg.

Notes

The authors declare no competing financial interest.

ACKNOWLEDGMENTS

This research was supported by the National Research Foundation, Prime Minister's Office, Singapore, under its Competitive Research Programme (CRP Award No. NRF-CRP 4-2008-06). We are also thankful to Professor Y. Lifshitz from Technion Israel Institute of Technology for fruitful discussions.

REFERENCES

(1) Richter, H. J. The Transition from Longitudinal to Perpendicular Recording. *J. Phys. D: Appl. Phys.* **2007**, *40*, R149−R177.

(2) Kryder, M. H.; Gage, E. C.; McDaniel, T. W.; Challener, W. A.; Rottmayer, R. E.; Ju, G.; Hsia, Y. T.; Erden, M. F. Heat Assisted Magnetic Recording. *Proc. IEEE* **2008**, *96*, 1810−1835.

(3) Rottmayer, R. E.; Batra, S.; Buechel, D.; Challener, W. A.; Hohlfeld, J.; Kubota, Y.; Lie, L.; Bin, L.; Mihalcea, C.; Mountfield, K.; Pelhos, K.; Peng, C. Heat-Assisted Magnetic Recording. *IEEE Trans. Magn.* **2006**, *42*, 2417−2421.

(4) Coffey, K. R.; Parker, M. A.; Howard, K. J. High Anisotropy $L1_0$ Thin Films for Longitudinal Recording. *IEEE Trans. Magn.* **1995**, *31*, 2737−2739.

(5) Thiele, J.-U.; Folks, L.; Toney, M. F.; Weller, D. K. Perpendicular Magnetic Anisotropy and Magnetic Domain Structure in Sputtered Epitaxial FePt (001) $L1_0$ Films. *J. Appl. Phys.* **1998**, *84*, 5686−5692.

(6) Ferrari, A. C. Diamond-Like Carbon for Magnetic Storage Disks. *Surf. Coat. Technol.* **2004**, *180−181*, 190−206.

(7) Bernhard, P.; Ziethen, Ch.; Ohr, R.; Hilgers, H.; Schönhense, G. Investigations of the Corrosion Protection of Ultrathin a-C And a-C:N Overcoats for Magnetic Storage Devices. *Surf. Coat. Technol.* **2004**, *180−181*, 621−626.

(8) Robertson, J. Ultrathin Carbon Coatings for Magnetic Storage Technology. *Thin Solid Films* **2001**, *383*, 81−88.

(9) Zhang, H.-S.; Komvopoulos, K. Surface Modification of Magnetic Recording Media by Filtered Cathodic Vacuum Arc. *J. Appl. Phys.* **2009**, *106*, 093504.

(10) Rismani, E.; Samad, M. A.; Sinha, S. K.; Yeo, R.; Yang, H.; Bhatia, C. S. Ultrathin Si/C Graded Layer to Improve Tribological Properties of Co Magnetic Films. *Appl. Phys. Lett.* **2012**, *101*, 191601.

(11) Bhatia, C. S.; Anders, S.; Brown, I. G.; Bobb, K.; Hsiao, R.; Bogy, D. B. Ultra-Thin Overcoats for the Head/Disk Interface Tribology. *J. Tribol.* **1998**, *120*, 795−799.

(12) Yeo, R. J.; Rismani, E.; Dwivedi, N.; Blackwood, D. J.; Tan, H. R.; Zhang, Z.; Tripathy, S.; Bhatia, C. S. Bi-Level Surface Modification of Hard Disk Media by Carbon Using Filtered Cathodic Vacuum Arc: Reduced Overcoat Thickness Without Reduced Corrosion Performance. *Diamond Relat. Mater.* **2014**, *44*, 100−108.
(13) Joshi, A.; Nimmagadda, R.; Herrington, J. Oxidation Kinetics of Diamond, Graphite, and Chemical Vapor Deposited Diamond Films by Thermal Gravimetry. *J. Vac. Sci. Technol. A* **1990**, *8*, 2137−42.
(14) Wang, N.; Komvopoulos, K.; Rose, F.; Marchon, B. Structural Stability of Hydrogenated Amorphous Carbon Overcoats Used in Heat-Assisted Magnetic Recording Investigated by Rapid Thermal Annealing. *J. Appl. Phys.* **2013**, *113*, 083517.
(15) Jones, P. M.; Ahner, J.; Platt, C. L.; Tang, H.; Hohlfeld, J. Understanding disk Carbon Loss Kinetics for Heat Assisted Magnetic Recording. *IEEE Trans. Magn.* **2014**, *50*, 3300704.
(16) Wang, N.; Komvopoulos, K. Thermal Stability of Ultrathin Amorphous Carbon Films for Energy-Assisted Magnetic Recording. *IEEE Trans. Magn.* **2011**, *47*, 2277−2282.
(17) Du, Z.; Sarofim, A. F.; Longwell, J. P.; Mims, C. A. Kinetic Measurement and Modeling of Carbon Oxidation. *Energy Fuels* **1991**, *5*, 214−221.
(18) Pathem, B. K.; Guo, X.-C.; Rose, F.; Wang, N.; Komvopoulos, K.; Schreck, E.; Marchon, B. Carbon Overcoat Oxidation in Heat-Assisted Magnetic Recording. *IEEE Trans. Magn.* **2013**, *49*, 3721−3724.
(19) Samad, M. A.; Xiong, S.; Pan, L.; Yang, H.; Sinha, S. K.; Bogy, D. B.; Bhatia, C. S. A Novel Approach of Carbon Embedding in Magnetic Media for Future Head/Disk Interface. *IEEE Trans. Magn.* **2012**, *48*, 1807.
(20) Kundu, S.; Gaur, N.; Saifullah, M. S. M.; Yang, H.; Bhatia, C. S. Spacer-less, Decoupled Granular $L1_0$ FePt Magnetic Media using Ar−He Sputtering Gas. *J. Appl. Phys.* **2012**, *112*, 113916.
(21) Yeo, R. J.; Dwivedi, N.; Rismani, E.; Satyanarayana, N.; Kundu, S.; Goohpattader, P. S.; Tan, H. R.; Srinivasan, N.; Druz, B.; Tripathy, S.; Bhatia, C. S. Enhanced Tribological, Corrosion, and Microstructural Properties of an Ultrathin (<2 nm) Silicon Nitride/Carbon Bilayer Overcoat for High Density Magnetic Storage. *ACS Appl. Mater. Interfaces* **2014**, *6*, 9376−9385.
(22) Wang, N.; Komvopoulos, K. Incidence Angle Effect of Energetic Carbon Ions on Deposition Rate, Topography, and Structure of Ultrathin Amorphous Carbon Films Deposited by Filtered Cathodic Vacuum Arc. *IEEE Trans. Magn.* **2012**, *48*, 2220−2227.
(23) Dwivedi, N.; Rismani, E.; Yeo, R. J.; Goohpattader, P. S.; Satyanarayana, N.; Srinivasan, N.; Druz, B.; Tripathy, S.; Bhatia, C. S. Probing the Role of an Atomically Thin SiNx Interlayer on the Structure of Ultrathin Carbon Films. *Sci. Rep.* **2014**, *4*, 5021.
(24) Ferrari, A. C.; Robertson, J. Resonant Raman Spectroscopy of Disordered, Amorphous, and Diamond-Like Carbon. *Phys. Rev. B* **2001**, *64*, 075414.
(25) Dwivedi, N.; Kumar, S.; Tripathi, R. K.; Carey, J. D.; Malik, H. K.; Dalai, M. K. Structural and Electronic Characterization of Nanocrystalline Diamondlike Carbon Thin Films. *ACS Appl. Mater. Interfaces* **2012**, *4*, 5309−5316.
(26) Zanin, H.; May, P. W.; Hamanaka, M. H. M. O.; Corat, E. J. Field Emission from Hybrid Diamond-like Carbon and Carbon Nanotube Composite Structures. *ACS Appl. Mater. Interfaces* **2013**, *5*, 12238−12243.
(27) Anders, S.; Ager, J. W.; Pharr, G. M.; Tsui, T. Y.; Brown, I. G. Heat Treatment of Cathodic Arc Deposited Amorphous Hard Carbon Films. *Thin Solid Films* **1997**, *308*−*309*, 186−190.
(28) Kalish, R.; Lifshitz, Y.; Nugent, K.; Prawer, S. Thermal Stability and Relaxation in Diamond-like Carbon: A Raman Study of Films with Different sp^3 Fractions (ta-C to a-C). *Appl. Phys. Lett.* **1999**, *74*, 2936.
(29) Ferrari, A. C.; Kleinsorge, B.; Morrison, N. A.; Hart, A.; Stolojan, V.; Robertson, J. Stress Reduction and Bond Stability during Thermal Annealing of Tetrahedral Amorphous Carbon. *J. Appl. Phys.* **1999**, *85*, 7191.
(30) Lifshitz, Y.; Kasi, S. R.; Rabalais, J. W. Subplantation Model for Film Growth from Hyperthermal Species. J. W. *Phys. Rev. B* **1990**, *41*, 10468.
(31) Robertson, J. Diamond-like Amorphous Carbon. *Mater. Sci. Eng. R* **2002**, *37*, 129−281.
(32) Balandin, A. A.; Shamsa, M.; Liu, W. L.; Casiraghi, C.; Ferrari, A. C. Thermal Conductivity of Ultrathin Tetrahedral Amorphous Carbon Films. *Appl. Phys. Lett.* **2008**, *93*, 043115.
(33) Ji, R.; Ma, Y.; Shakerzadeh, M.; Seet, H. L.; Hu, J. F. Laser Irradiation Effect on Carbon Overcoat for HAMR Application. *Surf. Interface Anal.* **2014**, DOI: 10.1002/sia.5551.
(34) Donnet, C.; Erdimir, A. *Tribology of Diamond-like Carbon Films: Fundamentals and Applications*, 16th ed.; Springer: New York, 2008.
(35) Lifshitz, Y. Pitfalls in Amorphous Carbon Studies. *Diamond Relat. Mater.* **2003**, *12*, 130−140.